

Backward Smoothing versus Fixed-Lag Smoothing in Particle Filters

Genshiro Kitagawa

Tokyo University of Marine Science and Technology
and
The Institute of Statistical Mathematics

February 17, 2026

Abstract

Particle smoothing enables state estimation in nonlinear and non-Gaussian state-space models, but its practical use is often limited by high computational cost. Backward smoothing methods such as the Forward Filter Backward Smoother (FFBS) and its marginal form (FFBSm) can achieve high accuracy, yet typically require quadratic computational complexity in the number of particles. This paper examines the accuracy–computational cost trade-offs of particle smoothing methods through a trend-estimation example. Fixed-lag smoothing, FFBS, and FFBSm are compared under Gaussian and heavy-tailed (Cauchy-type) system noise, with particular attention to $\mathcal{O}(m)$ approximations of FFBSm based on subsampling and local neighborhood restrictions. The results show that FFBS and FFBSm outperform fixed-lag smoothing at a fixed particle number, while fixed-lag smoothing often achieves higher accuracy under equal computational time. Moreover, efficient FFBSm approximations are effective for Gaussian transitions but become less advantageous for heavy-tailed dynamics.

Key words: Particle filter; Particle smoother; Backward smoothing; FFBSm; Fixed-lag smoothing; Computational complexity; Non-Gaussian state-space models

1 Introduction

State-space models provide a flexible and powerful framework for analyzing time-series data by explicitly separating the latent system dynamics from the observation mechanism. When the model is linear and Gaussian, optimal filtering and smoothing can be performed efficiently by the Kalman filter and fixed-interval smoother ([1]). However, many real-world phenomena exhibit nonlinear dynamics and non-Gaussian disturbances, for which closed-form solutions are no longer available ([13], [11]).

Sequential Monte Carlo methods, commonly referred to as particle filters and smoothers, were developed to address this limitation. By representing probability distributions with a finite set of random samples (particles), particle methods enable recursive filtering and smoothing for general nonlinear and non-Gaussian state-space models. Since their introduction, they have been successfully applied to a wide range of problems in signal processing, econometrics, and engineering ([4], [6], [9], [11]).

Despite their flexibility, particle smoothers suffer from intrinsic computational and statistical challenges. In particular, smoothing algorithms that rely on backward recursions often experience particle degeneracy, where only a small fraction of particles effectively contribute to the approximation ([4], [9]). Moreover, backward smoothing methods such as the Forward Filter Backward Smoother (FFBS) and its marginal version (FFBSm) incur a high computational cost, typically of order $\mathcal{O}(m^2)$ per time step, which severely limits their practical applicability for large particle numbers ([2]).

Several approaches have been proposed to alleviate these difficulties, including fixed-lag smoothing, backward simulation, and various $\mathcal{O}(m)$ approximations of FFBSm based on truncation, kernel approximations, or subsampling. Fixed-lag smoothing offers a computationally attractive alternative, but introduces a bias that depends on the chosen lag length. Approximate FFBSm methods aim to retain the statistical efficiency of backward smoothing while reducing computational complexity, yet their performance strongly depends on the structure of the state dynamics and the tail behavior of the system noise ([2], [9]).

The purpose of this paper is to empirically investigate the accuracy–computational cost trade-offs of particle smoothing methods through a simple but informative trend-estimation example. Focusing on a first-order trend model, we compare fixed-lag smoothing, FFBS, and FFBSm under Gaussian and heavy-tailed (Cauchy-type) system noise ([13], [9]). Special attention is paid to $\mathcal{O}(m)$ approximations of FFBSm based on subsampling and local neighborhood restrictions, and to how their effectiveness depends on the tail behavior of the transition distribution.

Although the numerical study is limited to a single class of models, it clearly illustrates the conditions under which fast particle smoothing methods can be effective, and when simpler alternatives such as fixed-lag smoothing are preferable under realistic computational constraints. The results provide practical guidance for selecting particle smoothing strategies in applications where both accuracy and computational efficiency are of concern.

The remainder of the paper is organized as follows. Section 2 briefly reviews filtering and smoothing algorithms for state-space models. Section 3 describes particle filters and smoothers, including FFBS, FFBSm, and their computationally efficient approximations. Section 4 presents the numerical experiments and discusses the key findings. Section 5 concludes with a summary and practical implications.

2 A Brief Review of the Filtering and Smoothing Algorithms

2.1 The state-space model and the state estimation problems

Consider a time series $\{y_n\}$ described by the linear state-space model

$$x_n = F_n x_{n-1} + G_n v_n, \quad (1)$$

$$y_n = H_n x_n + w_n, \quad (2)$$

where x_n is a k -dimensional state vector. The system noise v_n and the observation noise w_n are assumed to be ℓ -dimensional and one-dimensional white-noise sequences with density functions $q_n(v)$ and $r_n(w)$, respectively. The initial state vector x_0 is assumed to follow the density $p(x_0)$.

Let Y_j denote the set of observations up to time j , that is, $Y_j \equiv \{y_1, \dots, y_j\}$. The state estimation problem is to evaluate the conditional density $p(x_n | Y_j)$ of the state x_n given the observations Y_j and the initial density $p(x_0 | Y_0) \equiv p(x_0)$. When $n > j$, $n = j$, and $n < j$, the problem is referred to as prediction, filtering, and smoothing, respectively.

The linear state-space model (1)–(2) can be generalized to a nonlinear non-Gaussian state-space model of the form

$$\begin{aligned} x_n &= F_n(x_{n-1}, v_n), \\ y_n &= H_n(x_n) + w_n, \end{aligned} \quad (3)$$

where $F_n(\cdot, \cdot)$ and $H_n(\cdot)$ are possibly nonlinear functions of the state and the noise inputs. A wide variety of problems in time-series analysis can be formulated and analyzed using this nonlinear state-space framework ([13], [4]). This formulation can be further extended to a general state-space model defined directly through conditional distributions.

2.2 The Kalman filter and the smoother

When all noise densities $q_n(v)$ and $r_n(w)$, as well as the initial state density $p(x_0)$, are Gaussian, the conditional density $p(x_n | Y_m)$ associated with the linear state-space model (1)–(2) is also Gaussian. In this case, the mean vector and covariance matrix can be computed recursively using the Kalman filter and the fixed-interval smoothing algorithm ([1]).

Specifically, assume that $q_n(v) \sim N(0, Q_n)$, $r_n(w) \sim N(0, R_n)$, $p(x_0 | Y_0) \sim N(x_{0|0}, V_{0|0})$, and $p(x_n | Y_m) \sim N(x_{n|m}, V_{n|m})$. Then the Kalman filter is given as follows.

One-step-ahead prediction:

$$\begin{aligned} x_{n|n-1} &= F_n x_{n-1|n-1}, \\ V_{n|n-1} &= F_n V_{n-1|n-1} F_n^T + G_n Q_n G_n^T. \end{aligned} \quad (4)$$

Filtering:

$$\begin{aligned} K_n &= V_{n|n-1} H_n^T (H_n V_{n|n-1} H_n^T + R_n)^{-1}, \\ x_{n|n} &= x_{n|n-1} + K_n (y_n - H_n x_{n|n-1}), \\ V_{n|n} &= (I - K_n H_n) V_{n|n-1}. \end{aligned} \quad (5)$$

Using these filtering estimates, the smoothed density can be obtained by the fixed-interval smoothing algorithm ([1]).

Fixed-interval smoothing:

$$\begin{aligned} A_n &= V_{n|n} F_n^T V_{n+1|n}^{-1}, \\ x_{n|N} &= x_{n|n} + A_n (x_{n+1|N} - x_{n+1|n}), \\ V_{n|N} &= V_{n|n} + A_n (V_{n+1|N} - V_{n+1|n}) A_n^T. \end{aligned} \quad (6)$$

2.3 The non-Gaussian filter and the smoother

For the nonlinear non-Gaussian state-space model (3), the conditional densities of the one-step-ahead predictor, the filter, and the smoother satisfy the following recursive relations ([7]).

One-step-ahead prediction:

$$p(x_n | Y_{n-1}) = \int_{-\infty}^{\infty} p(x_n | x_{n-1}) p(x_{n-1} | Y_{n-1}) dx_{n-1}. \quad (7)$$

Filtering:

$$p(x_n | Y_n) = \frac{p(y_n | x_n) p(x_n | Y_{n-1})}{\int p(y_n | x_n) p(x_n | Y_{n-1}) dx_n}. \quad (8)$$

Smoothing:

$$p(x_n | Y_N) = p(x_n | Y_n) \int_{-\infty}^{\infty} \frac{p(x_{n+1} | Y_N) p(x_{n+1} | x_n)}{p(x_{n+1} | Y_n)} dx_{n+1}. \quad (9)$$

[7] and [?] proposed a numerical algorithm for implementing the non-Gaussian filter and smoother by approximating each density function with a step function or a continuous piecewise linear function and performing numerical integration. This approach has been successfully applied to a wide range of problems, including trend and volatility estimation, spectrum smoothing, smoothing of discrete processes, and tracking problems ([13]; [11]).

3 Particle Filter and Smoothers

The numerical-integration-based non-Gaussian filter and smoother reviewed in the previous section are limited in practice to low-dimensional state-space models, typically of third or fourth order. To overcome this limitation, sequential Monte Carlo filtering and smoothing methods, hereafter referred to as *particle filters*, were developed. In particle methods, each distribution appearing in the recursive filtering and smoothing equations is approximated by a collection of particles, which can be interpreted as random realizations from the corresponding distribution ([6]; [8]; [9]).

3.1 Forward Filter and Fixed-Lag Smoother

Consider the state-space model

$$x_n \sim p(x_n | x_{n-1}), \quad (10)$$

$$y_n \sim p(y_n | x_n), \quad (11)$$

where y_n denotes the observation and x_n the latent state. The objective of marginal smoothing is to approximate, for each time step n , the marginal posterior distribution

$$p(x_n | Y_N), \quad (12)$$

conditioned on the entire observation sequence $Y_N \equiv \{y_1, \dots, y_N\}$.

Forward filtering. In the forward pass, a particle filter approximates the filtering distribution as

$$p(x_n | Y_n) \approx \sum_{i=1}^m w_n^{(i)} \delta_{x_n^{(i)}}(x_n), \quad (13)$$

where $\{x_n^{(i)}, w_n^{(i)}\}_{i=1}^m$ denote the particles and their normalized weights. These are obtained recursively through prediction and update steps. The particle system at each time step is stored for use in subsequent smoothing procedures.

ESS-based resampling in forward filtering. As time progresses, the importance weights $\{w_n^{(i)}\}_{i=1}^m$ often become highly uneven, leading to weight degeneracy, in which only a small number of particles carry most of the probability mass. A commonly used diagnostic for this phenomenon is the effective sample size (ESS), defined by

$$\text{ESS}_n = \frac{1}{\sum_{i=1}^m (w_n^{(i)})^2}, \quad (14)$$

where the weights satisfy $\sum_{i=1}^m w_n^{(i)} = 1$. The ESS takes values in $[1, m]$, with smaller values indicating more severe degeneracy ([14]; [4]).

To mitigate degeneracy while avoiding unnecessary resampling, an ESS-based resampling strategy is employed. Specifically, resampling is performed only when

$$\text{ESS}_n < \alpha m, \quad (15)$$

where $\alpha \in (0, 1)$ is a user-specified threshold, typically chosen between 0.3 and 0.7. When ESS_n exceeds this threshold, resampling is skipped and the weighted particle system is propagated to the next time step.

When resampling is triggered, a new set of particles $\{x_n^{(i)}\}_{i=1}^m$ is generated by sampling with replacement from the current particles according to their weights $\{w_n^{(i)}\}_{i=1}^m$. After resampling, all particles are assigned equal weights $w_n^{(i)} = 1/m$. This adaptive strategy balances variance reduction and particle diversity and is therefore widely used in practical implementations of particle filters.

Fixed-lag smoothing. It is interesting that particles approximating a smoothing distribution can be obtained by a simple modification of the particle filter ([8]; [9]). Let $(s_{1|j}^{(i)}, \dots, s_{n|j}^{(i)})^T$ denote the i th realization from the conditional joint distribution $p(x_1, \dots, x_n | Y_j)$. A fixed-lag smoothing algorithm is obtained by replacing Step 2(d) of the filtering algorithm with the following procedure:

(d-S) Generate $\{(s_{n-L|n}^{(i)}, \dots, s_{n-1|n}^{(i)}, s_{n|n}^{(i)})^T, w_n^{(i)}\}$, $i = 1, \dots, m$, from the previous state vectors $\{(s_{n-L|n-1}^{(i)}, \dots, s_{n-1|n-1}^{(i)}, p_n^{(i)})^T, w_{n-1}^{(i)}\}$. If $\text{ESS}_n < \alpha m$, perform resampling of the state vectors.

This procedure corresponds to an L -lag fixed-lag smoother rather than a fixed-interval smoother ([1]). Increasing the lag L generally improves the approximation of $p(x_n | Y_{n+L})$ to $p(x_n | Y_N)$, but it may simultaneously degrade the quality of the particle representation of $p(x_n | Y_{n+L})$ due to path degeneracy ([9]). Since $p(x_n | Y_{n+L})$ often converges rapidly to $p(x_n | Y_N)$, it is usually recommended to choose L moderately.

3.2 Backward marginal smoothing (FFBSm)

The Forward Filter Backward Smoother in its marginal form (FFBSm) computes the smoothing distributions $p(x_n | Y_N)$ directly, without sampling complete state trajectories ([4]; [5]). The method is based on the identity

$$p(x_n | Y_N) = p(x_n | Y_n) \int \frac{p(x_{n+1} | x_n) p(x_{n+1} | Y_N)}{p(x_{n+1} | Y_n)} dx_{n+1}. \quad (16)$$

Using the particle approximation obtained from the forward filter and assuming

$$p(x_{n+1} | Y_N) \approx \sum_{j=1}^m \tilde{w}_{n+1}^{(j)} \delta_{x_{n+1}^{(j)}}(x_{n+1}), \quad (17)$$

the FFBSm recursion yields the following update for the smoothing weights:

$$\tilde{w}_n^{(i)} \propto w_n^{(i)} \sum_{j=1}^m \tilde{w}_{n+1}^{(j)} \frac{p(x_{n+1}^{(j)} | x_n^{(i)})}{\sum_{k=1}^m w_n^{(k)} p(x_{n+1}^{(k)} | x_n^{(i)})}, \quad i = 1, \dots, m. \quad (18)$$

After normalization, the weighted particles $\{x_n^{(i)}, \tilde{w}_n^{(i)}\}_{i=1}^m$ provide an approximation of $p(x_n | Y_N)$.

Computational complexity. The exact FFBSm recursion involves a double summation over particle indices and has computational complexity $\mathcal{O}(m^2 N)$, which can be prohibitive for large number of particles m . Consequently, FFBSm is often used as a benchmark or reference smoother.

Various approximation techniques have been proposed to reduce the computational cost, including local window truncation, kernel density approximations, and importance-sampling-based methods. These approaches reduce the complexity to

$$\mathcal{O}(mN) \quad \text{or} \quad \mathcal{O}(mm_s N), \quad (19)$$

where $m_s \ll m$ denotes the size of a local subsample, at the cost of introducing a controlled approximation error.

Discussion. Compared with backward-simulation-based smoothers (FFBSi), which generate full state trajectories, FFBSm directly targets marginal smoothing distributions and typically yields lower-variance estimates of marginal expectations. This property makes FFBSm particularly attractive for applications such as parameter estimation via EM algorithms and offline state estimation, where accurate marginal posterior distributions are required.

In summary, FFBSm provides a principled framework for marginal smoothing in particle filters, offering exact but computationally demanding formulations as well as efficient approximations that trade accuracy for scalability.

3.3 Subsampled FFBSm and Local Neighborhood Subsampling FFBSm

To reduce the computational cost of the marginal Forward Filter Backward Smoother (FFBSm), we consider two approximation strategies based on (i) truncating the state space using local neighborhoods and (ii) performing subsampling within each local neighborhood.

Simple subsampling. As a first step toward reducing the computational cost of FFBSm, we approximate the summation in equation (17) by evaluating it over a subset of indices. Specifically, instead of computing the sum over the full index set $J = \{1, \dots, m\}$, we restrict the summation to a subset $\{j_1, \dots, j_{m_s}\}$ of size m_s . For simplicity, we assume that $m_{\text{int}} = m/m_s$ is an integer.

Several straightforward strategies can be used to select m_s indices from J :

1. selecting m_s equally spaced indices according to $j_i = j_0 + (i - 1)m_{\text{int}}$;
2. partitioning the interval $[1, m]$ into m_s subintervals of length m_{int} and randomly sampling one index from each subinterval;
3. performing stratified sampling over J using the weights $w_n^{(k)}$.

In what follows, for the sake of simplicity, we focus on the first strategy based on equally spaced sampling. This approach is referred to as the *subsampled FFBSm (S-FFBSm)*.

Neighborhood definition. Let $V_n = x_{n+1} - x_n$ denote the state transition noise with cumulative distribution function F_V . For a prescribed tolerance level $\varepsilon > 0$, we define a distance threshold L_ε such that

$$\mathbb{P}(|V_n| > L_\varepsilon) = \varepsilon. \quad (20)$$

Given a particle $x_{n+1}^{(j)}$ at time $n+1$, the corresponding local neighborhood at time n is defined as

$$\mathcal{N}_n(j) = \left\{ k \in \{1, \dots, m\} : \|x_{n+1}^{(j)} - x_n^{(k)}\| \leq L_\varepsilon \right\}. \quad (21)$$

In this study, we set $\varepsilon = 1/m$, so that the number of particles m controls the target size of the neighborhood.

For light-tailed transition models, such as the Gaussian distribution, L_ε grows only logarithmically with m , resulting in highly localized neighborhoods. In contrast, for heavy-tailed transition models, such as the Cauchy distribution, L_ε increases approximately linearly with m , and the resulting neighborhood may cover a substantial portion of the state space. This difference reflects the fundamentally distinct tail behaviors of the two noise models.

Subsampling within the neighborhood. Even when the neighborhood $\mathcal{N}_n(j)$ is relatively large, additional computational savings can be achieved by approximating the summations in the FFBSm recursion using a small subset of indices. Specifically, for each j , we draw a subset

$$S_n(j) \subset \mathcal{N}_n(j), \quad |S_n(j)| = m_{\text{small}}, \quad (22)$$

either uniformly or according to a prescribed sampling distribution.

Using this subset, the denominator in the FFBSm update is approximated by

$$\hat{D}_j = \sum_{k \in S_n(j)} \frac{w_n^{(k)} p(x_{n+1}^{(j)} | x_n^{(k)})}{\pi_{jk}}, \quad (23)$$

where π_{jk} denotes the inclusion probability of index k in $S_n(j)$. When the indices are sampled uniformly from $\mathcal{N}_n(j)$, we have $\pi_{jk} = m_{\text{small}}/|\mathcal{N}_n(j)|$. This Horvitz–Thompson type estimator provides an unbiased estimate of the truncated denominator.

The smoothing weights are then updated according to

$$\tilde{w}_n^{(i)} \propto w_n^{(i)} \sum_{j=1}^m \tilde{w}_{n+1}^{(j)} \frac{p(x_{n+1}^{(j)} | x_n^{(i)}) \mathbf{1}\{i \in \mathcal{N}_n(j)\}}{\hat{D}_j}, \quad i = 1, \dots, m. \quad (24)$$

The same subsampling strategy can be applied to the numerator of the FFBSm recursion, yielding an approximate update of the smoothing weights. The resulting algorithm has computational complexity $\mathcal{O}(m m_{\text{small}} N)$, which is independent of the possibly large size of the neighborhood $\mathcal{N}_n(j)$. This approach is referred to as the *neighborhood subsampled FFBSm (NS–FFBSm)*.

Remark. For Gaussian transition models, the neighborhood $\mathcal{N}_n(j)$ is typically small, and the additional subsampling introduces only minor approximation error. For Cauchy transitions, the neighborhood may span most of the particle set; however, the subsampling step ensures that the computational cost remains well controlled. In this sense, the proposed approach provides a unified framework that adapts naturally to both light-tailed and heavy-tailed transition models while maintaining scalable computational complexity.

4 Example: Smoothing Accuracy of a Trend Model

4.1 Models and Evaluation Criterion

To evaluate the accuracy of particle smoothing distributions, we consider the following first-order trend model:

$$\begin{aligned} x_n &= x_{n-1} + v_n, \\ y_n &= x_n + w_n, \end{aligned} \quad (25)$$

where y_n is the observed time series, x_n is the trend component, v_n is the system noise, and w_n is the observation noise. We assume that the observation noise follows the Gaussian distribution $w_n \sim N(0, \sigma^2)$, and that the system noise follows either the Gaussian distribution $v_n \sim N(0, \tau^2)$ or the Cauchy distribution $v_n \sim C(0, \tau^2)$. Figure 1 shows the data set of length $N = 500$ used in the Monte Carlo experiments in this paper; the same data set was also used in [7], [9] and [10].

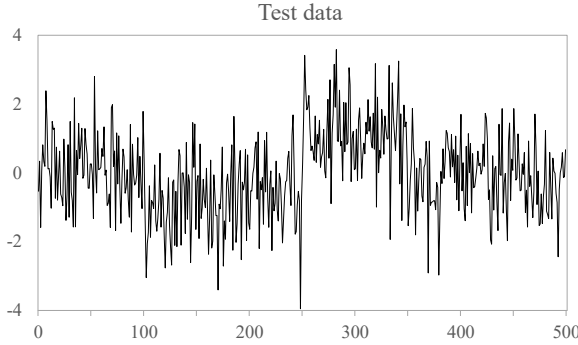


Figure 1: Test data used for the empirical study ([7], [9], [10]).

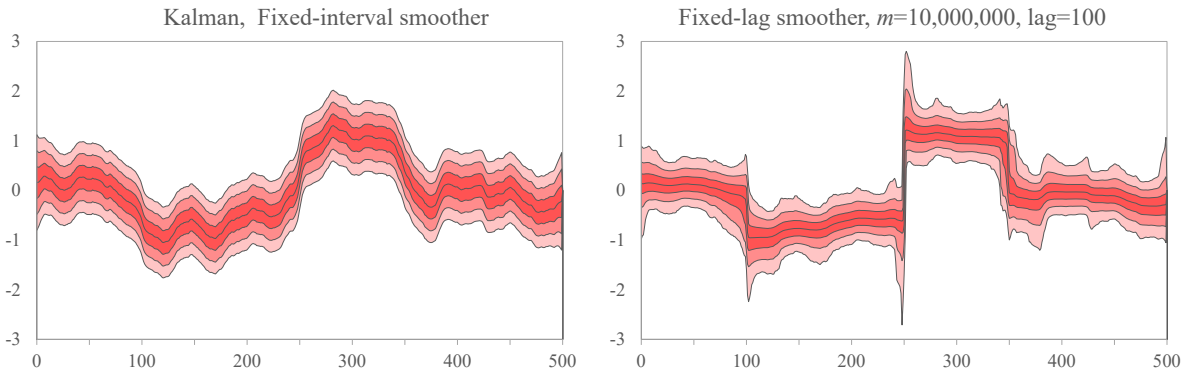


Figure 2: “True” smoothed distributions for the Gaussian and Cauchy models, obtained by the Kalman smoother and by a fixed-lag particle smoother with $m = 10,000,000$ particles, respectively.

Following [10], we evaluate the smoothed distributions using

$$\text{Dist}(D, \hat{D}) = \sum_{n=1}^{500} \sum_{i=1}^{6400} \left\{ D(x_i, n) - \hat{D}(x_i, n) \right\}^2 \Delta x, \quad (26)$$

where $D(x_i, n)$ and $\hat{D}(x_i, n)$ denote the “true” and estimated smoothed probability density functions at time n , evaluated on grid points x_i , $i = 1, \dots, 6400$. The grid is defined by $x_i = -8 + (i - 1)\Delta x$ with $\Delta x = 16/6400$.

Figure 2 displays the mean and the ± 1 to ± 3 standard-deviation bands of the “true” smoothed distributions for the Gaussian and Cauchy models. For the Gaussian model, the exact smoothing distribution is computed using the Kalman filter and fixed-interval smoother. For the Cauchy model, the “true” distribution is approximated by a fixed-lag particle smoother with 10^7 particles ([10]).

4.2 Fixed-lag Smoothing and FFBS

Table 1 reports the lag length that minimizes $\text{Dist}(D, \hat{D})$ for particle numbers $m = 10^k$, $k = 2, \dots, 7$ ([10]). For both models, the optimal lag increases with m . For the Gaussian model, the increase is moderate and a lag of around 50 is sufficient. For the Cauchy model, the optimal lag grows more rapidly with m and exceeds 100 when $m = 10^7$.

Table 1: Lag orders that minimize $\text{Dist}(D, \hat{D})$ for the fixed-lag smoother, relative to the “true” fixed-interval smoother.

m	10^2	10^3	10^4	10^5	10^6	10^7
Gaussian	16	22	27	32	43	53
Cauchy	17	28	48	80	93	108

Table 2: Accuracy of the smoothing distributions and CPU time for the fixed-lag smoother and FFBSm. The number of Monte Carlo repetitions is $\text{NSIM} = 100$. (FFBSm with $m = 100,000$ was performed only once.) Values in parentheses are standard deviations.

m	Gaussian model				Cauchy model			
	Accuracy		CPU time (s)		Accuracy		CPU time (s)	
	Fixed-lag	FFBSm	Fixed lag	FFBSm	Fixed-lag	FFBSm	Fixed lag	FFBSm
10^2	7.407(0.187)	5.269(0.201)	0.05	0.24	19.585(0.656)	15.135(0.600)	0.04	0.12
10^3	2.008(0.069)	1.074(0.062)	0.17	23.1	6.459(0.070)	2.816(0.151)	0.18	10.1
10^4	0.558(0.027)	0.191(0.010)	1.79	2535.	1.396(0.026)	0.208(0.011)	1.75	1027.
10^5	0.145(0.013)	0.006(—)	30.4	245222	0.137(0.003)	0.024(—)	51.7	112809
10^6	0.024(0.004)		551.		0.019(0.001)		1001.	
10^7	0.002(0.012)		8538		0.004(0.001)		18246	

Figure 3 and Table 2 summarize the estimation accuracy and computational time of fixed-lag smoothing and the Forward Filter Backward Smoother (FFBSm) for both the Gaussian and Cauchy models, as the number of particles is varied from 10^2 to 10^7 . Accuracy is evaluated by averaging $\text{Dist}(D, \hat{D})$ over 100 independent runs with different random seeds. For fixed-lag smoothing, the lag length is set to the optimal values in Table 1. All computations were performed on a PC equipped with an Intel Core i7-8700 CPU running at 3.20–4.30 GHz.

Table 2 suggests the following. First, the qualitative dependence of accuracy and computational time on m is similar for the Gaussian and Cauchy models. Second, both fixed-lag smoothing and FFBSm exhibit rapid improvement in accuracy as m increases, and FFBSm consistently achieves higher accuracy than fixed-lag smoothing for the same m . Third, the running time of FFBSm increases rapidly with m , reflecting its quadratic computational complexity $\mathcal{O}(m^2)$. Finally, when the methods are compared under the same computational time budget, fixed-lag smoothing often attains superior accuracy.

Panels (a) and (c) of Figure 3 show the relationship between accuracy and m for the Gaussian and Cauchy models, respectively. In both cases, the curves are approximately linear on a log–log scale. The FFBSm results (blue) lie below the fixed-lag results (red), indicating that FFBSm is more accurate at the same particle number.

Panels (b) and (d) compare accuracy against CPU time. Here, the relative ordering is reversed: under the same computational time budget, fixed-lag smoothing consistently achieves higher accuracy than FFBSm.

4.3 Effect of $\mathcal{O}(m)$ Approximation in FFBSm

As discussed above, the exact FFBSm algorithm is computationally prohibitive for large m . We therefore focus on FFBSm and representative $\mathcal{O}(m)$ approximation strategies.

Specifically, we consider the following three approximations for the summation in the FFBSm recursion:

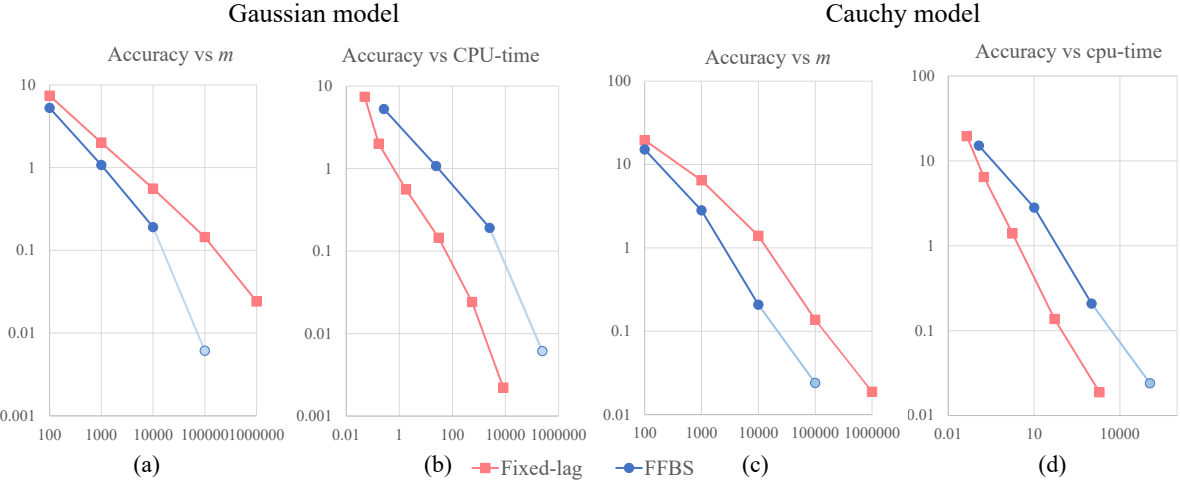


Figure 3: Smoothing accuracy comparison for the Gaussian model. (Left) Accuracy versus particle number m (FFBS and fixed-lag smoothing). (Right) Accuracy versus CPU time for the same experiments. FFBS with $m = 10^5$ is computed only once and hence denoted by light blue.

- (i) replacing the full summation over all indices by a sum over only m_s equally spaced indices;
- (ii) partitioning the index set $\{1, \dots, m\}$ into m_s subintervals and sampling one index within each subinterval (stratified sampling);
- (iii) identifying a local neighborhood first and then applying stratified sampling within that neighborhood.

The local neighborhood is defined according to the system noise model, which is either Gaussian or Cauchy. For each distribution, we determine $k = k_m$ such that

$$\mathbb{P}(|X| > k_m) = \frac{1}{m}. \quad (27)$$

When the system noise has variance (or dispersion) parameter τ^2 , the neighborhood associated with particle $x_{n+1}^{(j)}$ is defined as

$$\left[x_{n+1}^{(j)} - k_m \tau, \quad x_{n+1}^{(j)} + k_m \tau \right]. \quad (28)$$

Table 3: Values of k_m for Gaussian, Cauchy, and truncated Cauchy distributions.

m	Gaussian			Cauchy	Truncated Cauchy	
	k_m	\hat{k}_m	$k_m \tau_G$	k_m	\tilde{k}_m	$\tilde{k}_m \tau_{TC}$
10^2	2.5758	2.6630	0.2845	6.3657×10	6.137×10	0.3619
10^3	3.2905	3.3668	0.3635	6.3662×10^2	4.629×10^2	2.7302
10^4	3.8906	3.9593	0.4297	6.3662×10^3	1.339×10^3	7.8972
10^5	4.4172	4.4802	0.4879	6.3662×10^4	1.651×10^3	9.7406
10^6	4.8916	4.9502	0.5403	6.3662×10^5	1.691×10^3	9.9734

Table 3 reports the values of k_m and $k_m\tau$ for $m = 10^2, \dots, 10^6$ for the Gaussian, Cauchy, and truncated Cauchy distributions. For the Gaussian distribution, we also report the approximation

$$\hat{k}_m \sim \sqrt{2 \ln(2m) - \ln(\ln(2m)) - \ln(2\pi)}$$

(see [15]). For the truncated Cauchy distribution, the values \tilde{k}_m are obtained by Monte Carlo computation.

For the Gaussian distribution, k_m ranges approximately from 2.5 to 4.9. In our setting, the standard deviation of the Gaussian system noise is $\tau_G = \sqrt{0.0122} = 0.1105$, so $k_m\tau_G$ takes the values reported in Table 3. In contrast, for the Cauchy distribution, k_m increases rapidly with m , so that the neighborhood becomes too wide to substantially reduce the computational domain.

For the truncated Cauchy distribution with truncation limits ± 10 , Table 3 reports k_m and $k_m\tau_{TC}$. The values are obtained by Monte Carlo approximation. In this setting, k_m is small when $m = 100$, whereas for $m \geq 10^4$ it approaches 10, effectively corresponding to an untruncated range.

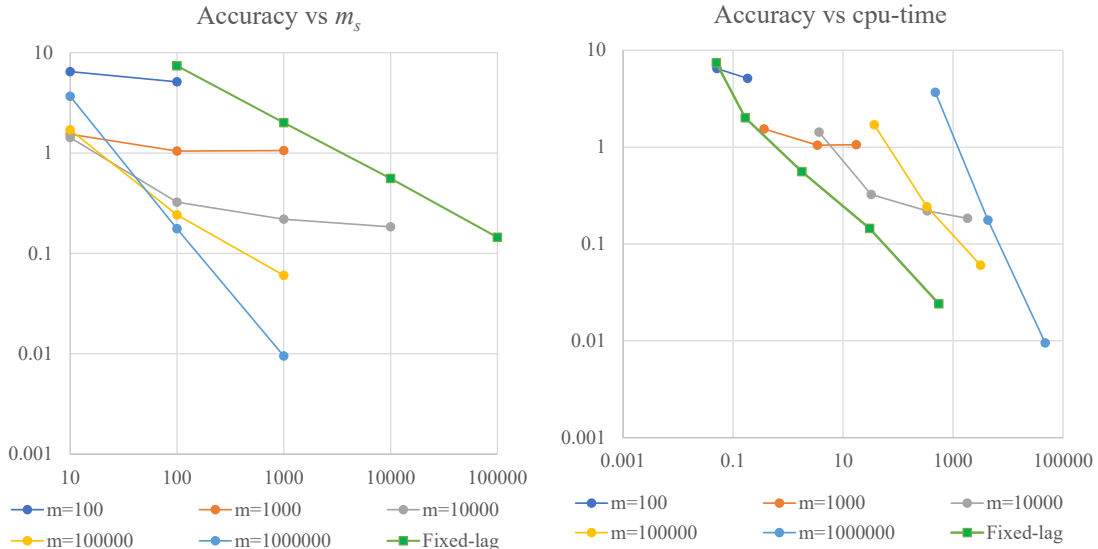


Figure 4: Smoothing accuracy for the Gaussian model. (Left) NS-FFBSm accuracy versus m_s for different particle numbers m , with fixed-lag smoothing shown for comparison. (Right) Accuracy versus CPU time for the same experiments.

Figure 4 illustrates the relationship between smoothing accuracy and the choices of m and m_s for the Gaussian model. Numerical values are reported in Table 4 in the Appendix. In the left panel, the horizontal axis represents m_s and the vertical axis shows the accuracy measure $\text{Dist}(D, \hat{D})$ for NS-FFBSm. The navy, red, gray, orange, and blue curves correspond to $m = 10^2, 10^3, 10^4, 10^5$, and 10^6 , respectively. For comparison, results for fixed-lag smoothing are also shown in green; in that case, the horizontal axis is the particle number m .

The NS-FFBSm accuracy curves become nearly flat when m_s is reduced to approximately $m/100$, indicating that further improvements are negligible beyond this point. This suggests that choosing m_s on the order of $m/100$ (or smaller) is sufficient in practice for Gaussian transitions. Fixed-lag smoothing is slightly less accurate than NS-FFBSm for each m , which is likely attributable to degeneracy induced by repeated resampling.

The right panel shows the same results plotted against CPU time. Under a fixed computational budget, fixed-lag smoothing (green curve) consistently achieves the best accuracy.

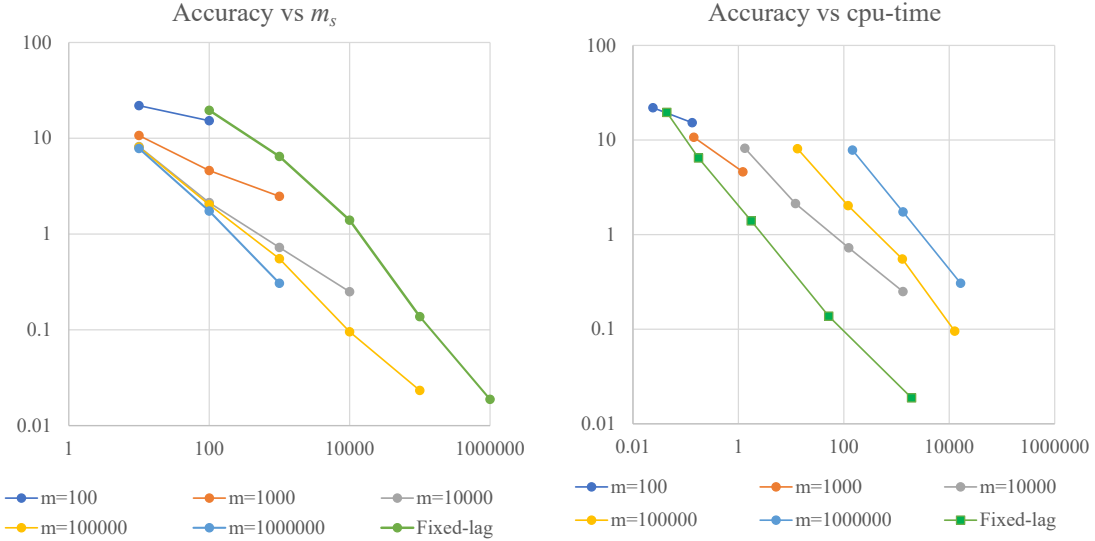


Figure 5: Smoothing accuracy for the truncated Cauchy model. (Left) Accuracy versus m_s on a log–log scale. (Right) Accuracy versus CPU time.

Although fixed-lag smoothing is less accurate than FFFBSm and NS-FFBFSm for the same m , it requires only resampling of stored particles during smoothing and therefore incurs relatively low additional cost. As a result, fixed-lag smoothing can use a larger m within the same time budget and outperforms FFFBSm and NS-FFBFSm in terms of accuracy under equal computational time.

Figure 5 presents the corresponding results for the truncated Cauchy model. Numerical values are reported in Table 5 in the Appendix. Unlike the Gaussian case, accuracy improves almost linearly with m_s on a log–log scale. This can be attributed to the fact that, except for very small m , the neighborhood interval effectively covers most of the state space for the Cauchy model. Consequently, accurately approximating the smoothing distribution requires larger m_s , and accuracy continues to improve as m_s increases. As in the Gaussian case, when $m_s = m$, FFFBSm is more accurate than fixed-lag smoothing for the same m , typically reducing the error by a factor of several.

The right panel plots accuracy against CPU time. Accuracy improves nearly linearly with computational time, and the curves are approximately equally spaced. Under the same computational budget, the choice $m_s = m$ achieves the highest accuracy. In this setting as well, fixed-lag smoothing can attain comparable or higher accuracy under equal CPU time by employing a larger number of particles.

Overall, Gaussian transitions allow efficient smoothing through strong localization, so that FFFBSm can achieve high accuracy with relatively small m_s . In contrast, heavy-tailed Cauchy transitions hinder localization and require larger m_s for substantial accuracy gains. Fixed-lag smoothing, although less accurate than FFFBSm-based methods at a fixed particle number, often achieves superior accuracy under equal computational time due to its substantially lower computational cost.

4.4 Posterior Distributions Obtained by FFFBSm

In this subsection, we present illustrative examples of the posterior distributions of the trend estimated by NS-FFBFSm or S-FFBFSm.

Figure 6 shows NS-FFBFSm results for the Gaussian model using the local neighborhood $\mathcal{N}_t(j)$, for $m = 100, 1000$, and $10,000$, with $m_s = 10, \dots, m$. Even for the smallest configuration

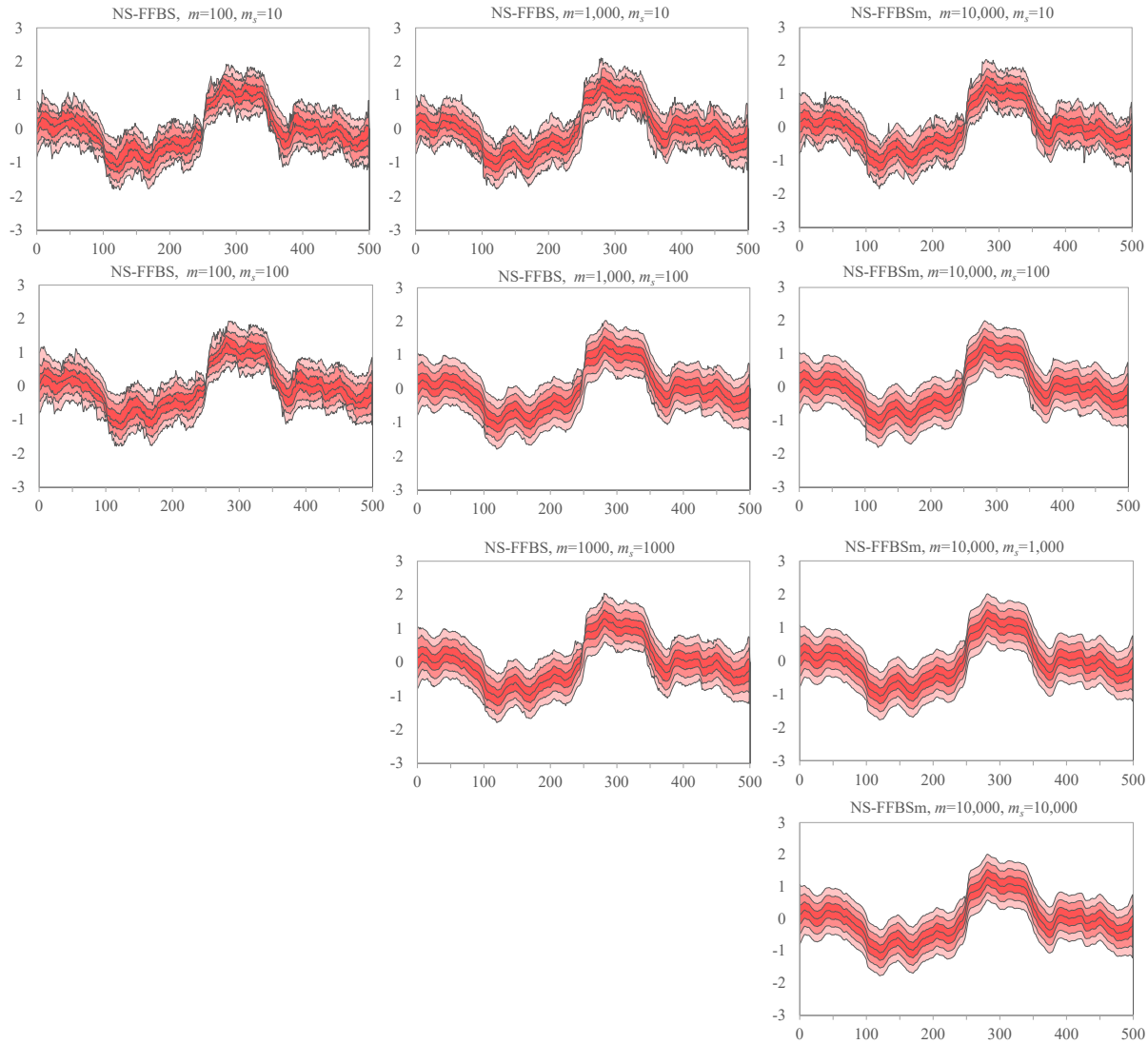


Figure 6: Posterior distributions of the trend estimated by NS-FFBSm for the Gaussian model using local neighborhoods $\mathcal{N}_t(j)$. Results are shown for $m = 100, 1000$, and $10,000$ with $m_s = 10, \dots, m$, including the posterior mean and the ± 1 , ± 2 , and ± 3 standard-deviation curves.

$(m = 100, m_s = 10)$, both the posterior mean and the ± 1 to ± 3 standard-deviation bands are estimated reasonably well. In particular, for $m \geq 1000$ and $m_s \geq 100$, the results are comparable to those obtained with $m = m_s = 10,000$ (bottom-right panel), indicating no noticeable loss in estimation quality.

Figure 7 shows S-FFBSm results for the Cauchy model. In contrast to the Gaussian case, trend jumps are not well captured when $m = 100$. Moreover, even for larger m , noticeable irregularities and unnatural discontinuities appear in the outer confidence bands when $m_s = 10$. Nevertheless, when $m \geq 1000$ and $m_s \geq 100$, the estimated posterior distributions improve substantially. In particular, $m = 10,000$ with $m_s = 100$ is sufficient to obtain a reliable approximation in these experiments.

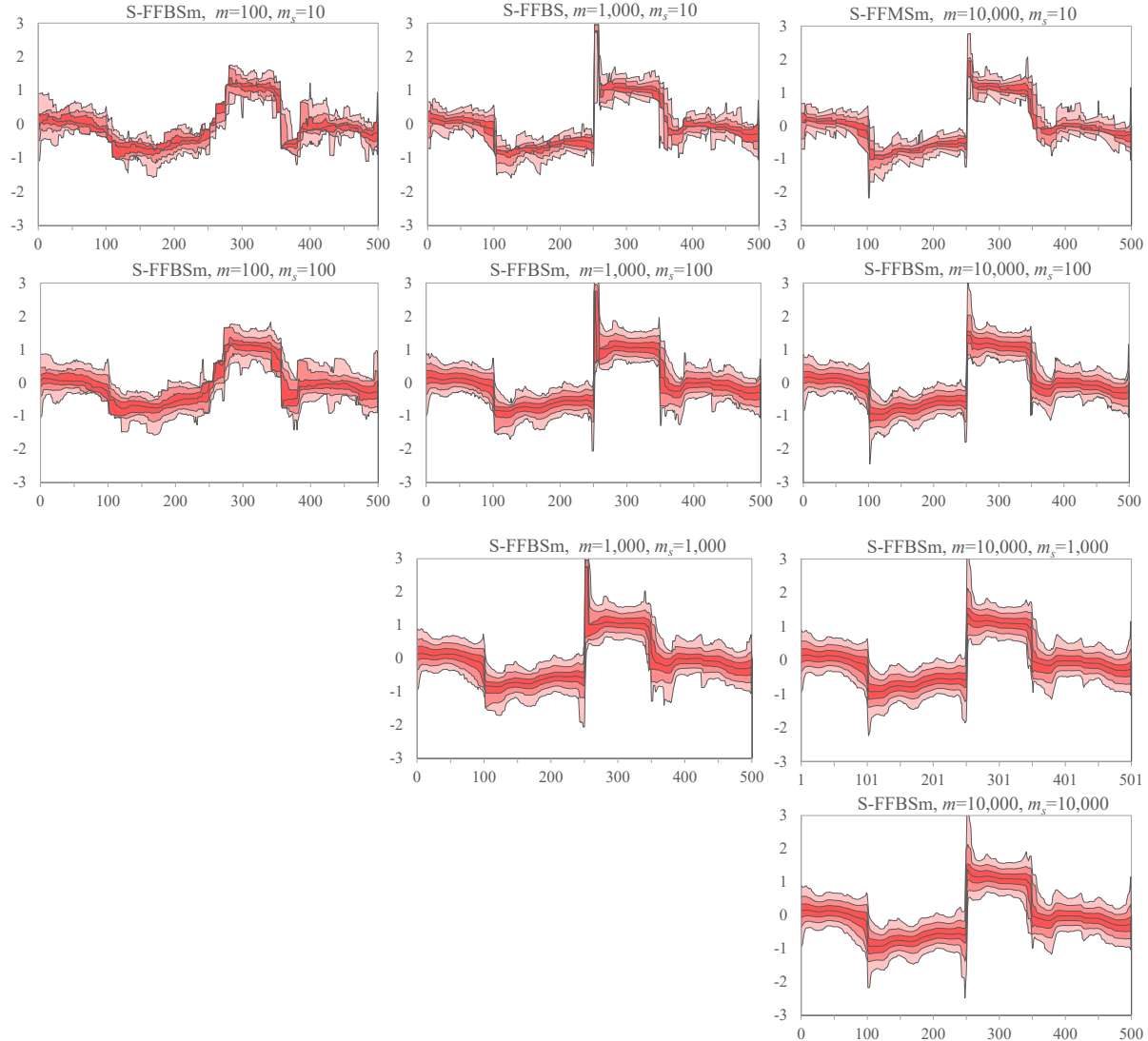


Figure 7: Posterior distributions of the trend estimated by S-FFBSm for the Cauchy model. Results are shown for different particle numbers m and subsample sizes m_s , illustrating the effect of heavy-tailed system noise on the estimated posterior distributions.

5 Conclusion

This paper investigated, through a trend-estimation example, the practical accuracy–cost trade-offs of particle smoothing algorithms, with particular emphasis on backward marginal smoothing (FFBSm) and its computationally efficient approximations based on subsampling and local neighborhoods.

The experiments lead to the following main conclusions.

1. **Accuracy versus particle number.** For both Gaussian and heavy-tailed (truncated Cauchy) transition models, the smoothing error measure $\text{Dist}(D, \hat{D})$ decreases rapidly as the number of particles m increases. At a fixed particle number, FFBSm/LS-FFBSm consistently achieves smaller error than fixed-lag smoothing, reflecting the advantage of using information from the full data set in a principled backward recursion.
2. **Cost dominates method ranking under equal CPU time.** Despite its higher accuracy at fixed m , FFBSm (and exact FFBS) becomes computationally prohibitive as m increases due to its quadratic complexity. When methods are compared under the same computational time budget, fixed-lag smoothing often attains higher accuracy because it allows substantially larger particle numbers within the same runtime. This illustrates that the practical choice of smoother should be driven by computational constraints rather than by asymptotic accuracy alone.
3. **Localization is decisive for efficient FFBSm.** For Gaussian transitions, local neighborhoods are strongly localized, and NS-FFBSm accuracy becomes nearly insensitive once the subsample size m_s reaches a small fraction of m (on the order of $m/100$ in the present study). Hence, substantial computational savings are possible without noticeable loss of accuracy by combining FFBSm with neighborhood restriction and subsampling.
4. **Heavy tails hinder localization and require larger m_s .** For the (truncated) Cauchy transition model, the effective neighborhood typically spans a large portion of the particle cloud, and the accuracy continues to improve as m_s increases. In this regime, aggressive subsampling degrades the approximation, and the benefits of S-FFBSm approximations are limited unless m_s is chosen sufficiently large.
5. **Practical guidance.** Taken together, these results suggest a simple rule of thumb: when the state transition is light-tailed (e.g., Gaussian), FFBSm with local neighborhoods and modest subsampling can provide an accurate and computationally efficient smoother; when the transition is heavy-tailed, fixed-lag smoothing with a larger particle number may be preferable under a fixed computational budget.

Overall, the single trend-estimation example clearly demonstrates that the effectiveness of fast particle smoothing hinges on whether the dynamics admit meaningful localization. Extending these findings to higher-dimensional models and to other forms of state dynamics is an important direction for future work.

References

- [1] Anderson, B.D.O., and Moore, J.B. (1979). *Optimal Filtering*, New Jersey, Prentice-Hall.
- [2] Briers, M., Doucet, A. and Maskell, S., (2010). Smoothing algorithms for state-space models, *Annals of the Institute of Statistical Mathematics*, **62**, 61–89.
- [3] Doucet, A., Godsill, S. and Andrieu, C. (2000). On sequential Monte Carlo sampling methods for Bayesian filtering, *Statistics and Computing*, **10**, 197–208.
- [4] Doucet, A., de Freitas, N., and Gordon, N., (2001). *Sequential Monte Carlo Methods in Practice*. Springer-Verlag, New York.
- [5] Godsill, S., Doucet, A. and West, M., (2012). Monte Carlo smoothing for nonlinear time series. *Journal of the American Statistical Association* **99**(465), 156–168.
- [6] Gordon, N. J., Salmond, D. J., and Smith, A. F. M., (1993). Novel approach to nonlinear/non-Gaussian Bayesian state estimation, *IEE Proceedings-F*, **140**, 107–113.
- [7] Kitagawa, G. (1987), Non-Gaussian State Space Modeling of Nonstationary Time Series, *Journal of American Statistical Association*, **76**(400), 1032-1064.
- [8] Kitagawa, G., (1993). A Monte Carlo filtering and smoothing method for non-Gaussian nonlinear state space models, *Proceedings of the 2nd U.S.-Japan Joint Seminar on Statistical Time Series Analysis*, 110–131.
- [9] Kitagawa, G., (1996). Monte Carlo filter and smoother for non-Gaussian nonlinear state space model, *Journal of Computational and Graphical Statistics*, **5**, 1–25.
- [10] Kitagawa, G., (2014). Computational aspects of sequential Monte Carlo filter and smoother. *Annals of the Institute of Statistical Mathematics*, **66**, 443–471.
- [11] Kitagawa, G., (2020). *Introduction to Time Series Modeling with Applications in R*, Chapman & Hall/CRC Press, New York.
- [12] Kitagawa, G. (2024). Empirical Study on the Effect of Multi-Sampling in the Prediction Step of the Particle Filter. *arXiv preprint arXiv:2405.09167*.
- [13] Kitagawa, G., and Gersch, W., (1996). *Smoothness Priors Analysis of Time Series*, Springer-Verlag, New York.
- [14] Liu, J. S. and Chen, R., (1998). Sequential Monte Carlo Methods for Dynamic Systems. *Journal of the American Statistical Association*, **93**(443), 1032–1044.
- [15] Voutier, P.M., (2010). A New Approximation to the Normal Distribution Quantile Function, *arXiv:1002.0567*.

A Appendix

Table 4: Accuracy and cpu-time of Filter Distribution and Smoothing Distribution by Fixed-lag Smoothing and Backward Smoother. Gaussian distribution case. The values in parentheses indicate the standard deviation.

m	m_s	Accuracy			Cpu time			
		Fixed-lag	FFBSm	S-FFBSm	NS-FFBSm	Fixed-lag	FFBSm	S-FFBSm
10^2	10	(0.187)	(0.200)	9.347	6.476	0.05	0.24	0.04
	10^2	7.407	5.269	5.350	5.127			0.05
10^3	10			5.653	1.541	0.17	23.13	0.27
	10^2	(0.069)	(0.062)	1.556	1.047			2.49
	10^3	2.008	1.074	1.028	1.059			3.42
10^4	10			5.248	1.428	1.78	2535.	2.57
	10^2			0.947	0.324			24.84
	10^3	(0.027)	(0.010)	0.299	0.219			243.6
	10^4	0.558	0.191	0.2197	0.184			338.1
10^5	10			5.210	1.701	30.48	245222	26.33
	10^2			0.849	0.242			36.93
	10^3			0.135	0.060			257.83
	10^4	(0.013)	(—)	0.041	0.057			335.2
	10^5	0.144	0.006					3235.
10^6	10			3.679	3.877	551.06	38117.	3160.
	10^2			0.176	0.188			33571.
	10^3	(0.004)		0.010	0.009			325453.
	10^6	0.024						47347.

Table 5: Accuracy and cpu-time of Filter Distribution and Smoothing Distribution by Fixed-lag Smoothing and Backward Smoother. Truncated Cauchy distribution case. The values in parentheses indicate the standard deviation.

m	m_s	Accuracy			Cpu time			
		Fixed-lag	FFBSm	S-FFBSm	Fixed-lag	FFBSm	S-FFBSm	
10^2	10	(0.656)	(0.600)	21.916(0.804)	0.04	0.12	0.13	0.02
	10^2	19.585	15.135	15.2465(0.552)				
10^3	10			10.688(0.287)	0.18	10.11	13.45	0.14
	10^2	(0.230)	(0.151)	4.603(0.218)				1.22
	10^3	6.459	2.816	2.477(0.128)				
10^4	10			8.315(0.072)	1.75	1027.70	1325.23	1.33
	10^2			2.128(0.059)				12.13
	10^3	(0.026)	(0.010)	0.673(0.032)				123.94
	10^4	1.396	0.208	0.250(0.014)				
10^5	10			8.000(0.045)	51.74	101319	130620	13.21
	10^2			1.959(0.041)				120.63
	10^3			0.552(0.102)				1291.27
	10^4	(0.003)	(—)	0.087(0.014)				12705.0
	10^5	0.137	0.024	0.023(—)				
10^6	10			7.822(0.084)	1001.12	16409.00	146.17	
	10^2			1.738(0.036)				1328.69
	10^3	(0.001)		0.306(0.059)				
	10^6	0.019						16409.00